DETERMINATION OF SPACE SHUTTLE FLOW FIELD BY THE THREE-DIMENSIONAL METHOD OF CHARACTERISTICS

By Chong-Wei Chu and S.A. Powers

Northrop Corporation, Hawthorne, California

INTRODUCTION

Northrop's approach to the three-dimensional method of characteristics (3DMoC) has evolved over the last ten years (Refs. 1 to 7). Its fundamentals and initial formulation are discussed in References 1 to 3. Recently, the first author (CWC) has extensively revised and improved the numerical method and the computer program. The result is a new 3DMoC program that is accurate, efficient, and versatile, as verified by the excellent agreement between computed results and experimental data for a variety of bodies. This paper discusses the application of this method to space shuttle flow fields including wing-body interactions.

Basically, the Northrop approach follows streamlines from one data surface to the next and uses the redundant method to solve the compatibility relations (Ref. 3). All data surfaces are normal to a selected axis, usually the longitudinal body axis. The data rings on each data surface and the data points along each data ring are automatically respaced whenever their distribution becomes appreciably uneven. Provisions are made for automatic addition of data rings and for changing the number of data points per data ring at prescribed intervals. In addition, grid size variation can be related to the body geometry and flow-property gradients; for instance, smaller grid sizes can be specified near the wing tip and the wing-body junction. The step size (distance between two adjacent data surfaces) is automatically regulated by applying the Courant-Friedrichs-Lewy stability condition. The program also uses newly developed shock-point and body-point procedures, which eliminate most of the troublesome iterations. Very importantly, a shock stabilization technique has been developed to control shock point drift and thus maintain numerical stability even under adverse conditions. Realistic configurations can be easily treated by this program which uses a body description technique based on aircraft lofting practice.

The new program has been applied successfully to the calculation of flow fields over a variety of bodies including slab delta wings and shuttle orbiters. Flow fields over fuselage shapes for Mach numbers as low as 1.5 have been calculated. Some typical results are presented here.

CENTERLINE PRESSURE DISTRIBUTION ON SLAB DELTA WINGS
(Figure 1)

We have selected the computed pressure distribution on two slab delta wings as examples of the program's capabilities. Figure 1 shows the centerline pressure distribution on the windward side. At the left is a plot of local static pressure (non-dimensionalized by total pressure) against the distance along the windward surface centerline for a 70° slab delta wing at a free stream Mach number of 9.6 and at angles of attack of 0°, 4.5° and 15°. The computed pressure distributions are compared with experimental data of Bertram (Ref. 8). The comparison is excellent except for one point on each curve. At the right side of Figure 1 is a plot of the centerline pressure distribution on the windward side of an 80° sweep slab delta wing at 30° angle of attack, compared with experimental data of Whitehead (Ref. 9). Again, there is only slight difference between the computed pressure and the measured pressure. The curvature discontinuity at the junction of the spherical nose and the flat surface causes the wiggles which become more pronounced as the angle of attack increases. The computing time for 0 and 4.5° angle of attack cases was about 3 minutes on the CDC 6600 (including input and output), while for the 15° and 30° cases it was approximately 8 minutes.

CENTERLINE PRESSURE DISTRIBUTION ON SLAB DELTA WINGS

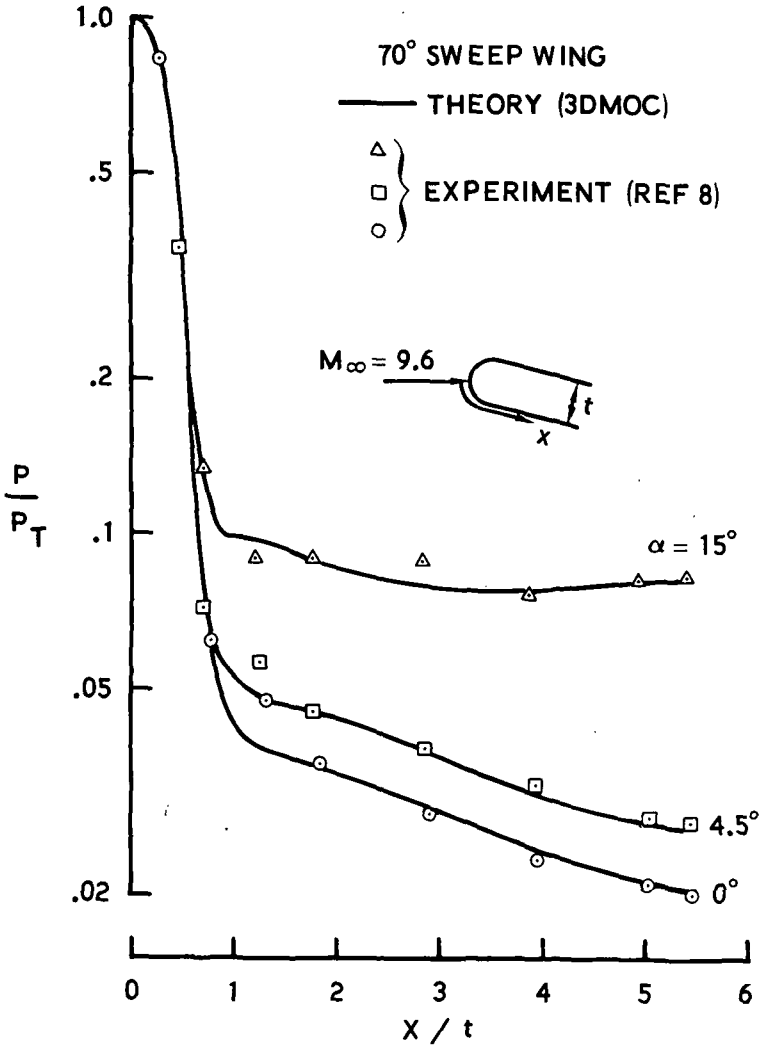

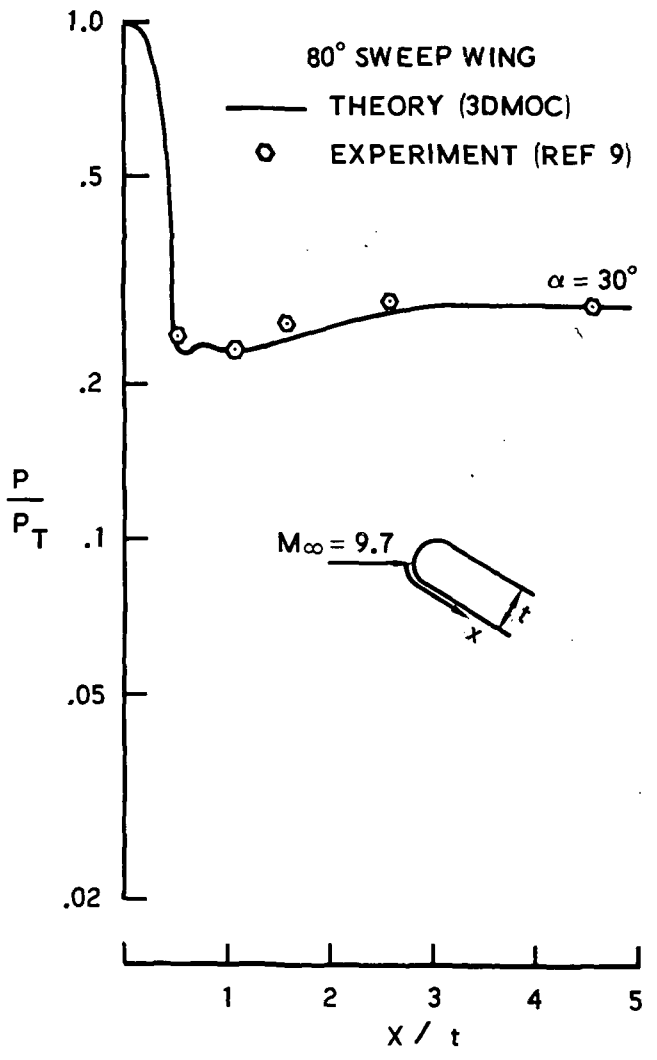

Figure 1

TRANSVERSE PRESSURE DISTRIBUTION ON SLAB DELTA WINGS
(Figure 2)

Typical transverse pressure distributions for the same two delta wings are shown in Figure 2. At the left is a plot of the local pressure (non-dimensionalized by the free stream pressure) at station L/t = 5 versus surface distance for the 70° sweep wing at 15° angle of attack. Positive S/t is the distance from the leading edge along the windward surface; negative S/t, along the leeward surface. Note that the maximum pressure occurs on the windward surface near the leading edge. The experimental data of Ref. 8 are again used for comparison. The agreement is excellent on the windward side. On the leeward side the agreement is surprisingly good except in the region near the leading edge. This indicates that the viscous effects play a secondary role in determining the surface pressure distribution even on the leeside at this angle of attack. At the right is a similar plot for the 80° sweep wing at 30° angle of attack, as compared with experimental data of Ref. 9. The agreement is again quite good except near the leading edge. It is possible that the discrepancy near the leading edge could be reduced by using a finer mesh size in the region of the leading edge.

TRANSVERSE PRESSURE DISTRIBUTION ON SLAB DELTA WINGS

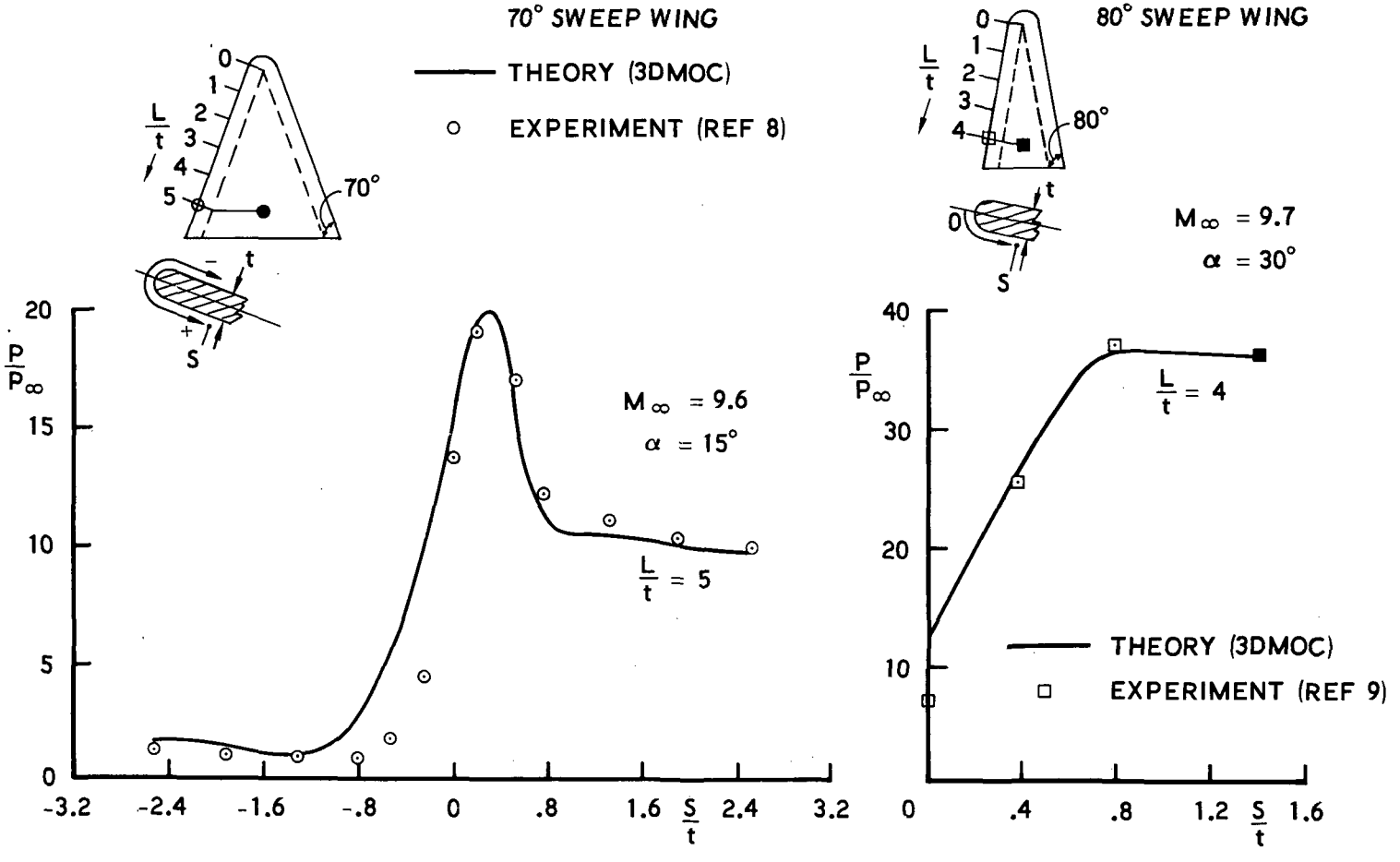

Figure 2

A SHUTTLE ORBITER AND COMPUTED SHOCK SHAPES
(Figure 3)

Our present method can handle very general smooth shuttle bodies. Figure 3 shows a shuttle orbiter and the computed shock shapes at Mach 5 and angles of attack of 5° and 20°. The body is described analytically. The upper profile, the lower profile, the maximum half breadth line and the wing leading edge are described by general conic equations in segments. The cross-section is described by an ellipse from a to b, a straight line from b to c, a cubic from c to d, and finally another ellipse from d to e. A realistic shuttle configuration can be described analytically in a similar way. Two cross-sections are noted for later use. Section C-C is located where the wing begins to emerge from the body and section D-D is located at the inflection point of the wing leading edge, which at that point makes a maximum angle of 32° with the body axis. Flow properties at these two sections will be discussed later.

At 5° angle of attack the bow shock, shown by dashed line, is well-behaved. At 20° angle of attack the bow shock, shown by the solid line, develops a kinked cross-section at the last station. However, as will be shown later, no such kink is observed at section D-D, even though the maximum local pressure, the maximum cross flow and the strongest embedded shock occur near section D-D. Nor was any kinked shock cross-section evident in the case of slab delta wings at high angles of attack. Thus, we believe that the kink is due to the added expansion caused by the curving back of the wing leading edge.

The location of the embedded shock is estimated by noting rapid changes of pressure gradients in the flow field. Even at 20° angle of attack, the embedded shock was weak and no provision for entropy change was made in the computation. The 5° angle of attack case took approximately 9 minutes of CDC 6600 time, while the 20° angle of attack case required approximately 35 minutes.

A SHUTTLE ORBITER AND COMPUTED SHOCK SHAPES

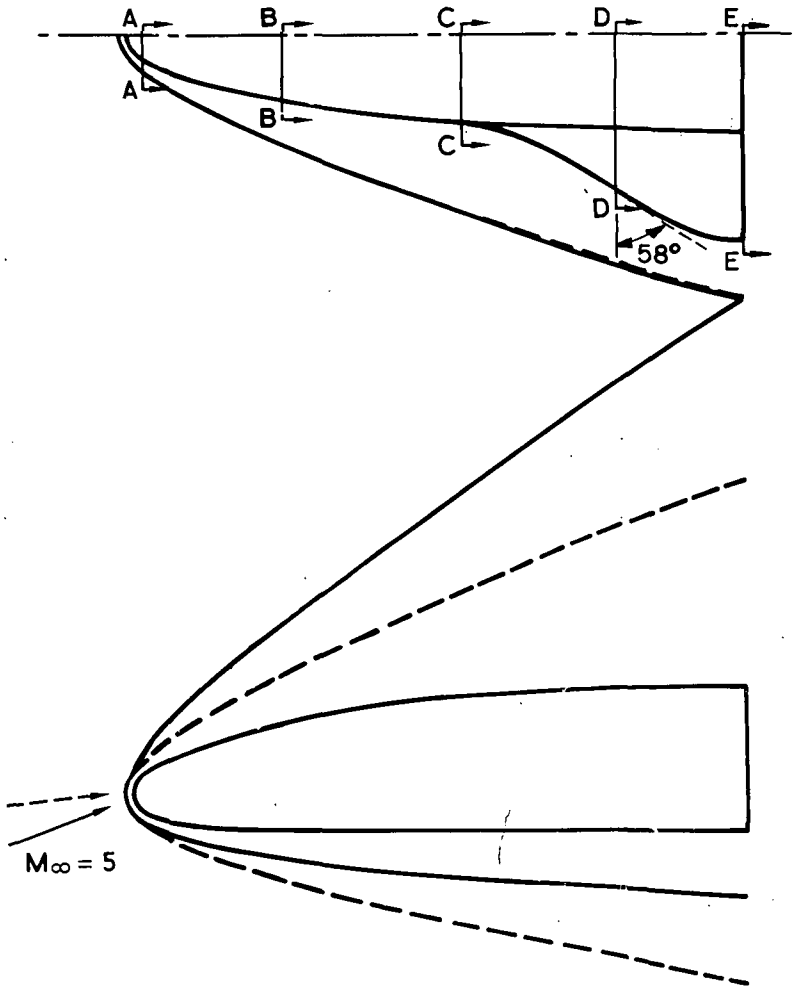

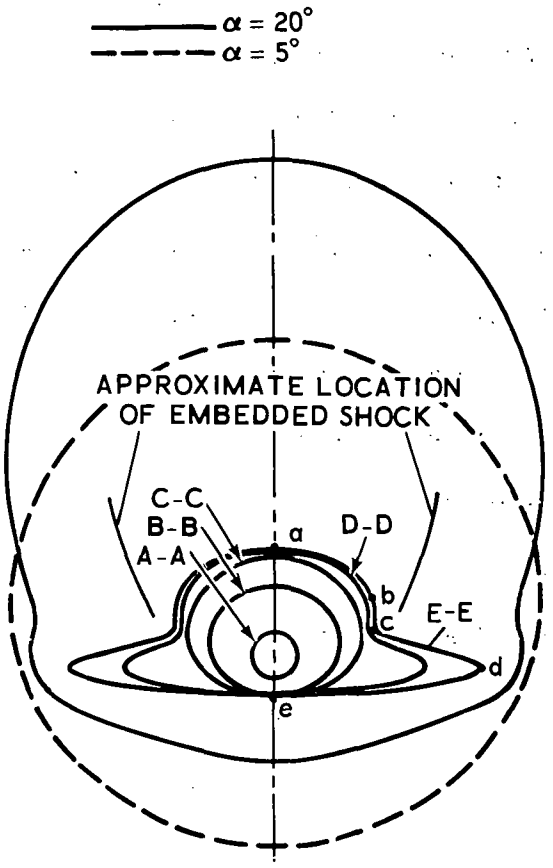

Figure 3

COMPUTED PRESSURE DISTRIBUTION ON WINDWARD SURFACE (Figure 4)

Figure 4 shows the pressure distribution on the windward surface and the associated cross-sections of the orbiter at $M_\infty = 5$ and $\alpha = 20°$. On the left are 5 cross-sections of the orbiter, and on the right is the plan view of the orbiter along with pressure plots corresponding to each cross-section. Along the centerline the pressure first decreases from the nose and then recovers somewhat. This recovery is apparently due to the widening of the windward surface in the winged portion of the orbiter. Along the wing leading edge the pressure attains a maximum near the 4^{th} section (Section D-D in Figure 3), at which the leading edge makes a maximum angle of 32° with the body axis. At each station in the winged portion of the orbiter, the pressure attains a maximum near the wing leading edge, just as in the case of the slab delta wing at 15° angle of attack. As the wing leading edge curves back, the maximum pressure drops rapidly. It is worth noting that the local Mach number attained a minimum of 1.25 at the maximum-pressure point and the computation went through without any problem.

COMPUTED PRESSURE DISTRIBUTION ON WINDWARD SURFACE

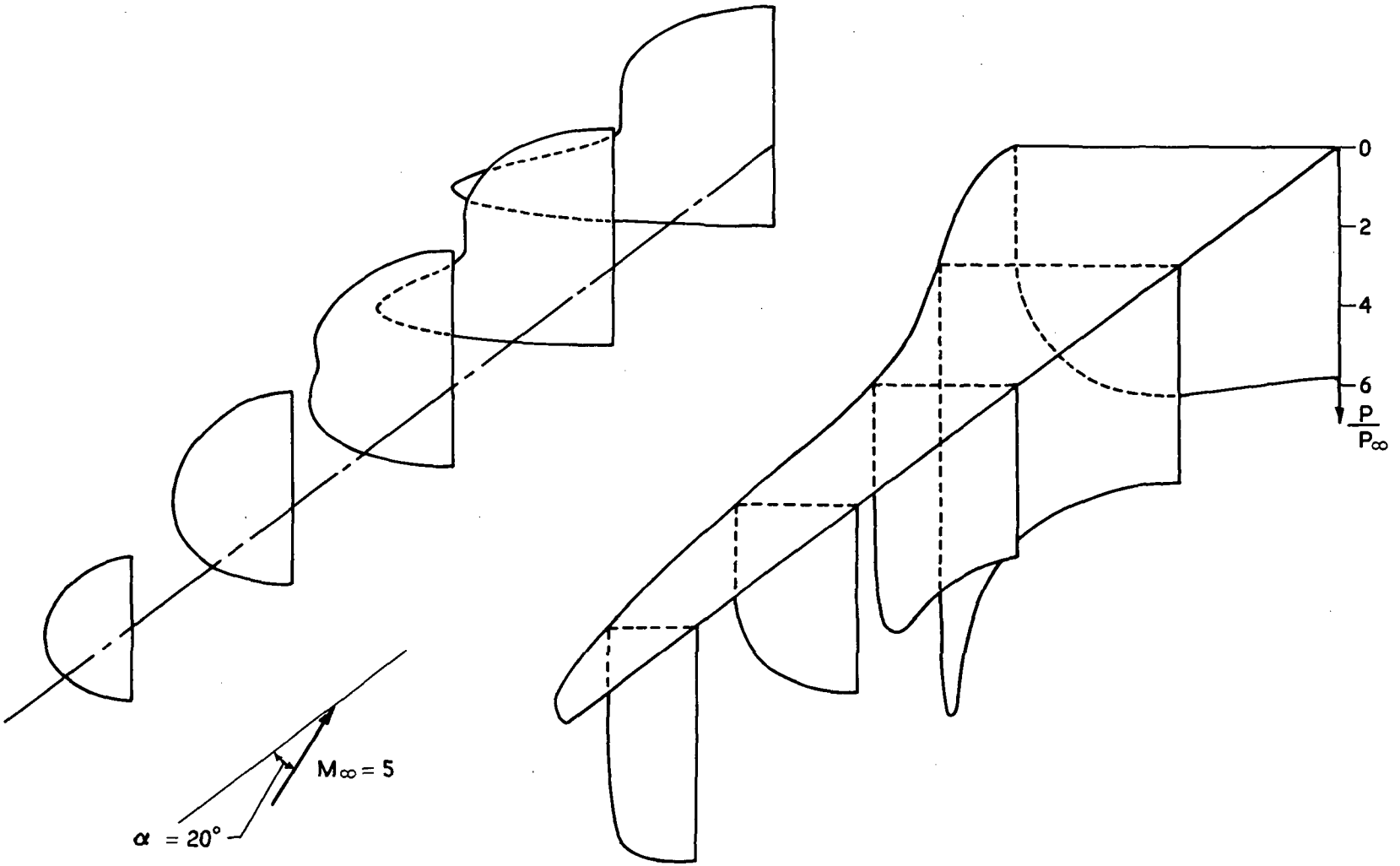

Figure 4

COMPUTED PRESSURE DISTRIBUTION ON LEEWARD SURFACE (Figure 5)

Figure 5 shows the leeward surface pressure distributions, which are continuations of those shown in Figure 4. Along the centerline the pressure first drops because of the continued expansion from the nose; the pressure then rises owing to the recompression created by the converging flow toward the plane of symmetry on the leeside. Since the flow is continually expanding from the windward side, the highest pressure on the leeward surface occurs along the leading edge. At 20° angle of attack considerable cross flow exists on the leeside. At the wing-body junction the cross flow generates a series of compression waves as shown by the pressure peak of the pressure curve. Actually the pressure spike is due to the method of plotting; there exists only a pressure bump as can be seen from the next figure.

COMPUTED PRESSURE DISTRIBUTION ON LEEWARD SURFACE

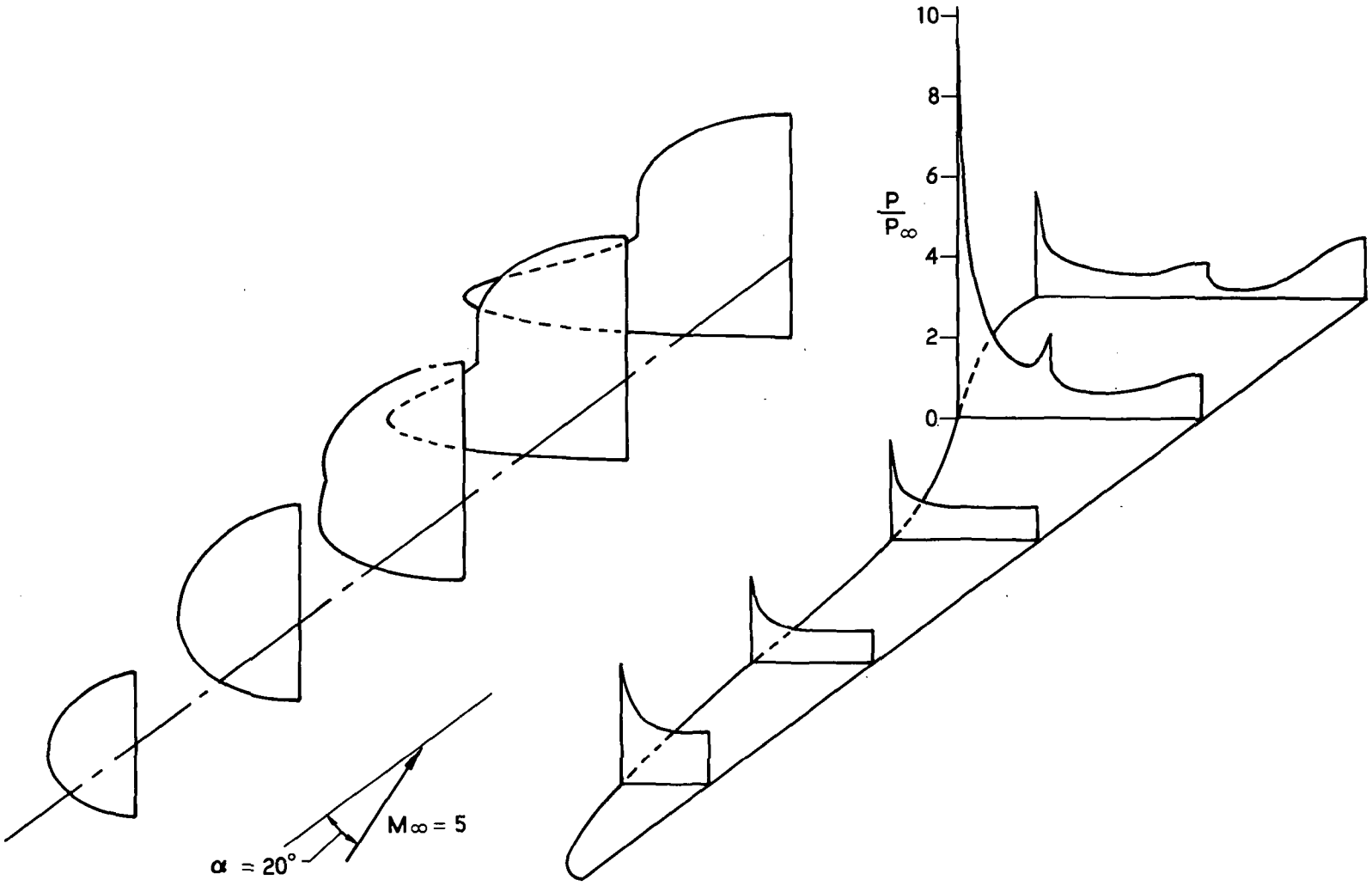

Figure 5

POLAR GRAPH OF PRESSURE DISTRIBUTION
(Figure 6)

Figure 6 is a polar plot of pressure distribution at section C-C and D-D. Section C-C is located where the wing is about to emerge from the body and section D-D is located where the wing leading edge makes a maximum angle with the body axis. At section C-C the pressure drops smoothly from the windside to the leeside, as might be expected. At section D-D, however, the pressure curve exhibits three peaks between the windward and leeward centerlines. The first peak occurs just below the wing tip where the combined effect of increasing wing span and high angle of attack causes the pressure to rise. The second peak at the wing-body junction is generated by the cross flow impinging on the upper body. The third peak at the leeside centerline of the orbiter is created by the flow converging toward the plane of symmetry. The second peak, which consists of a series of compression waves, is responsible for generating a weak embedded shock in the flow field. This pressure peak is the spike shown in the previous figure. It is interesting to note that the shape of the pressure distribution bears some resemblance to the body contour at both sections.

In order to define the local gradients in this complex flow field accurately, it was necessary to halve the grid size from the wing tip to the wing-body junction, and to halve it again in the region of the wing-body juncture.

POLAR GRAPH OF PRESSURE DISTRIBUTION

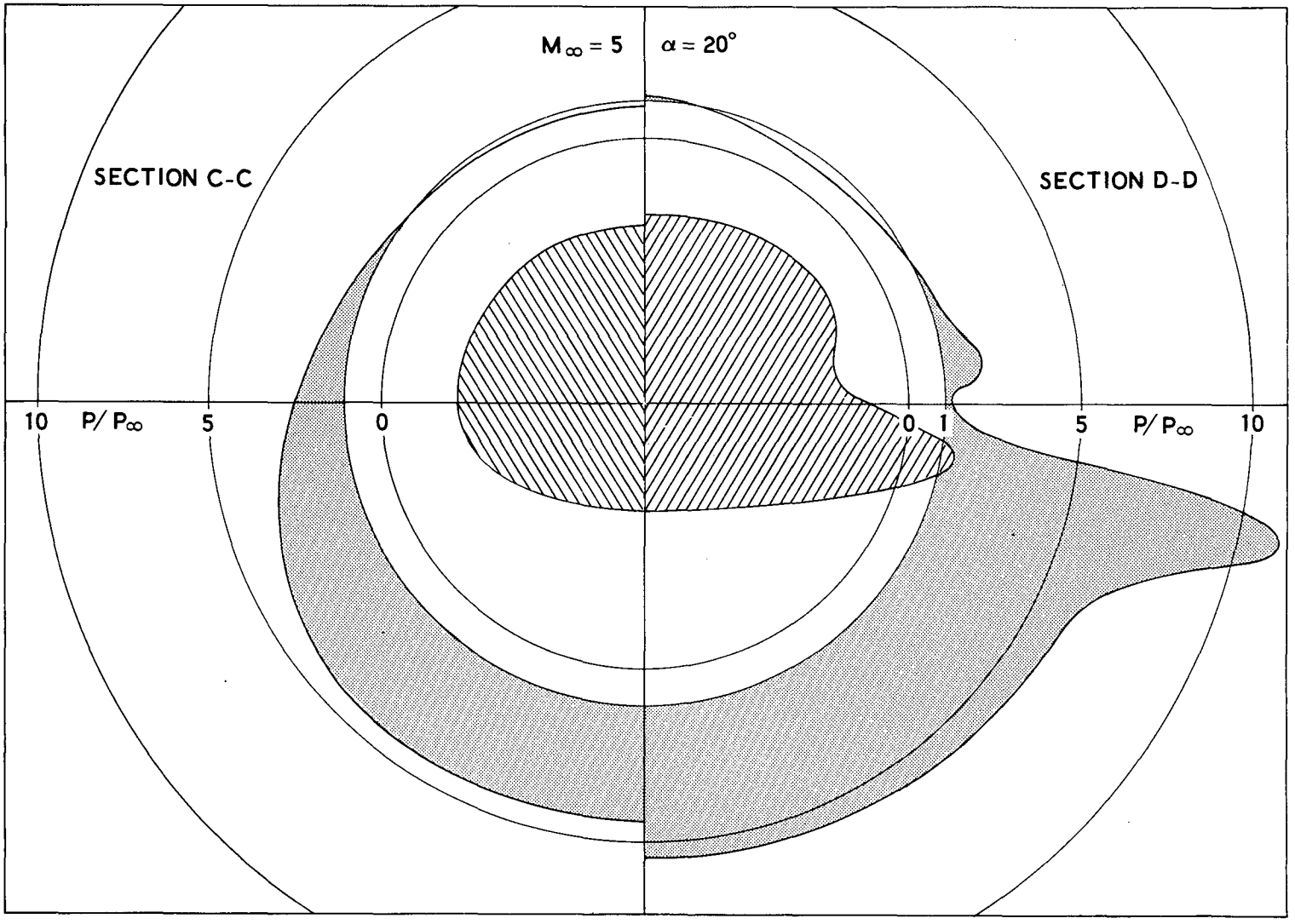

Figure 6

LOCAL FLOW DIRECTIONS
(Figure 7)

The local flow directions are shown in Figure 7, which is a plot of the projections of local unit velocity vectors on sections C-C and D-D. These arrows can be interpreted as velocity components normalized by the local speed.

The cross flow patterns are similar in both sections except in the region of the wing where the flow is greatly disturbed. As expected, large changes in the flow direction occur near the wing tip and considerable cross flow occurs near the wing root. It is this cross flow that generated the recompression observed as the second pressure peak in the preceding figure. The arrows are in general not tangent to the cross-sections because the axial velocity components are absent; the velocity is tangent to the body in three dimensions. For the same reason, the flow appears to move out of the shock on the leeside.

PROJECTIONS OF LOCAL UNIT VELOCITY VECTORS

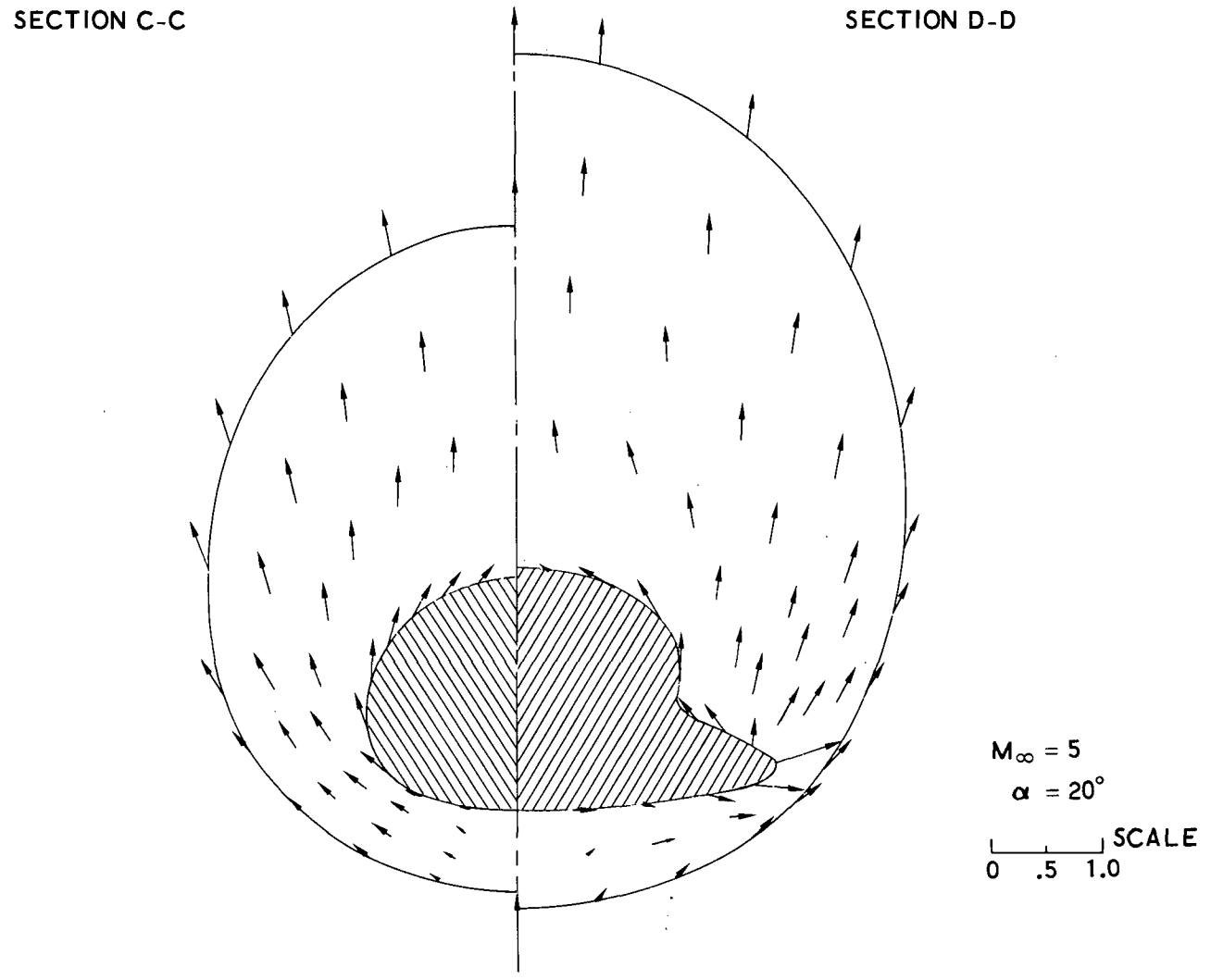

Figure 7

CONCLUSION

We have shown that Northrop's Three-Dimensional Method of Characteristics program is suitable for determining flow fields over space shuttle vehicles. Realistic configurations can be handled by this program if slope discontinuities on the body surfaces are smoothed out. However, this restriction will be removed in future developments. Configurations with thinner wings than those of the computed example will need more data points and correspondingly longer computer time, but they cause no fundamental difficulties. As long as the flow is supersonic and suitable initial value surfaces are obtained, this program can be used to determine the flow fields over realistic shuttle configurations even at high angles of attack.

REFERENCES

1. Fowell, L. R., "Solution of the starting region for the method of characteristics in general three-dimensional flow and solution of conical flows without symmetry," Northrop Report NOR 61-62 (1961).

2. Fowell, L. R., "The calculation of flow properties in a general three-dimensional field, a method of characteristics," Northrop Report NOR 61-65 (1961).

3. Chu, C. W., "Compatibility Relations and a Generalized Finite Difference Approximation for Three-Dimensional Steady Supersonic Flow," AIAA J. 5, 493-501 (1967).

4. Powers, S. A., Niemann, A. F. Jr. and Der, J. Jr., "A numerical procedure for determining the combined viscid-inviscid flow fields over generalized three-dimensional bodies," Air Force Flight Dynamics Laboratory Rept. AFFDL-TR-67-124 (1967).

5. Pridmore Brown, B. N. and Franks, W. J., "A method of characteristics solution in three independent variables," Aerospace Research Laboratories Report ARL 65-124 (1965).

6. Chu, C. W. and Ziegler, H., "Calculation of multiple rocket engine exhaust plumes by the method of characteristics," Northrop Report NOR 69-71 (1969).

7. Powers, S. A. and Beeman, E. R., Jr., "Flow fields over sharp-edge delta wings with attached shock," NASA CR-1738, (1971).

8. Bertram, M. H. and Everhart, P. E., "An experimental study of the pressure and heat transfer distribution on a 70° sweep slab delta wing in hypersonic flow," NASA TR-153 (1963).

9. Whitehead, A. H., "A study of the pressure and heat transfer distribution on a highly swept slab delta wing in hypersonic flow," Master Thesis, University of Virginia (1966).